ES98B Group Project - Tiangong Falling

Aditya Dugar • Ashleigh Shambrook • Andre Bittencourt • Harsh Raj • Stefan Zhikharev • Yuhan Zhang

Supervised by Dr Michael Faulkner

May 16, 2024

Abstract

The project focuses on utilising an Extended Kalman Filter to predict the impact location of a de-orbiting satellite undergoing uncontrolled re-entry into Earth's atmosphere. As the satellite's orbit decays, ground-based radar stations provide intermittent positional data for trajectory estimation. Gravitational forces and atmospheric drag are pivotal factors influencing the descent. The results demonstrate the effectiveness of Kalman filtering techniques in accurately predicting satellite trajectories, with initial covariance values quickly converging to precise estimates upon receiving observational data. Strategic utilisation of line-of-sight calculations ensures computational efficiency by focusing on radars within the satellite's visibility, enhancing prediction accuracy amidst dynamic operational conditions.

Keywords: Satellite, De-orbit, Modelling, Extended Kalman Filter, Prediction, Simulation

1 Introduction

In an era where space activities are increasingly prevalent, the safe re-entry of satellites at the end of their operational lifespan is of paramount importance. This project delves into the intricate task of predicting the impact location of a de-orbiting satellite as it hurtles towards Earth's surface. Ground-based radar stations, acting as vigilant sentinels, intermittently track the satellite's position, offering essential data for trajectory estimation. At the heart of this endeavour lies the utilisation of the Extended Kalman Filter (EKF), a powerful tool in the realm of predictive modelling, to refine the estimate of the satellite's landing site. This simulation project comprises two interlinked components: a sophisticated predictor, adept at assimilating radar measurements and continuously refining its predictions, and a simulator tasked with generating synthetic radar data to feed into the predictor.

The project's baseline model generates a scenario with the satellite de-orbiting from an equatorial orbit, closely observed by base stations along the equator. This foundational model employs fixed parameters

for the satellite's mass, drag coefficient, and atmospheric conditions, providing a solid starting point for exploration. However, the project's scope goes further than the baseline modelling. Advanced features are introduced to inject realism into the simulation, with elements such as non-equatorial orbits and non-equidistant radar locations. These enhancements aim to mirror the complexities of the real-world, thereby enriching the predictive accuracy of the model.

2 Background and Theory

This project works under the assumption of a constant mass and a cross-sectional area of the satellite taking the approximate values for the Tiangong space station from [5] and outlined in Table 2 alongside Earth's constants in Table 1.

Earth		
Mass, M_E (kg)	Principle Semi-Axis, (m)	
	Major, r_e	Minor, r_p
5.9722e24	6378136.6	6356751.9

Tab. 1 Earth Constants

Satellite	
Mass, m_S (kg)	Area, A_S (m^2)
8506	41.8

Tab. 2 Satellite Constants

2.1 Governing Equations

Main forces acting upon the satellite:

- A force in the direction of the centre of the Earth with magnitude $\frac{Gm_S M_E}{r^2}$, where G is the gravitational constant, r is the radius of the trajectory, and m_S, M_E are masses of the satellite and Earth.
- Atmospheric drag occurring in opposite direction of motion $F_D = \frac{1}{2}\rho v^2 C_d A_S$, for air density ρ, velocity v, drag coefficient C_d and effective satellite area A_S.

By defining the motion of the satellite within its orbital inclination plane centred on Earth centre, the equations of its motions in polar coordinates formulated by Nwankwo and Chakrabarti [4] are chosen for the orbital dynamics within this program. These equations are a suitable model for the position, velocity and acceleration of a satellite in a low Earth orbit, with the inclusion of atmospheric drag opposing its motion.

$$\dot{r} = v_r \tag{1}$$

$$\ddot{r} = -\frac{GM_E}{r^2} + r\dot{\theta}^2 \tag{2}$$

$$\dot{\theta} = \frac{v_\theta}{r} \tag{3}$$

$$\ddot{\theta} = -\frac{1}{2} B\, r\, \rho(h)\, \dot{\theta}^2 \tag{4}$$

Where v_r is radial velocity, v_θ is tangential velocity, θ is the polar angle measured from the z axis aligned with equatorial plane and B is the ballistic coefficient $\frac{A_S C_d}{m_S}$. These 2D orbital dynamics can be easily

translated into a 3 dimensional space through a particular choice of spherical coordinates axes.

2.2 Coordinate Systems

To allow for the implementation of the 2 dimensional orbital dynamic equations outlined in Section 2.1 it is necessary to define two sets of 3 dimensional modified spherical coordinate axes.

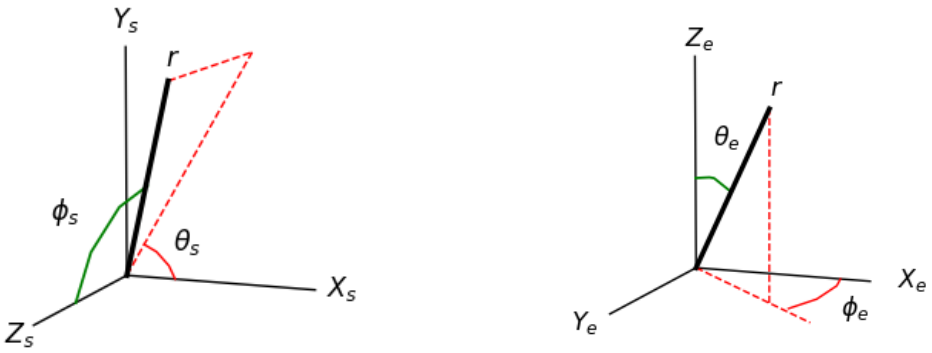

(a) Satellite Coordinates axes

(b) Earth Coordinates axes

Fig. 1 Modified spherical coordinate axes for the satellite and Earth planes in the same orientation

Figure 1 shows the two chosen axes systems, one defined for the dynamics of the satellite and the latter for Earth and its rotation, in the corresponding orientations. The satellite's system is designed with the z-axis aligned with Earth's equator, it solves the governing differential equation outlined in 2.1 within its r and polar angle ϕ_s. The inclination of the orbit is set by a constant azimuthal angle θ_S in this axes, rotating the orbital plane around the z-axis (Figure 1a). Earth takes the modified spherical coordinate system with Z_S aligned with the north and south poles, leaving x and y on the equator. This allows for the rotation of Earth around its poles to be a contained change in the Earth's azimuthal angle ϕ_E, with the altitude of a reference point being defined by its polar angle θ_E.These superimposed axes systems are calibrated around the initial position of the satellite being on both x axes. This translates computationally to an initial position of 0 rad in the azimuthal angle of Earth's system and an initial $\frac{\pi}{2}$ rad in the polar angle of the satellite's system.

2.3 Ellipsoidal Earth

While the shape of the Earth appears to be spherical from a distance it is actually an irregularly shaped ellipsoid, due to the bulge around the equator caused by the centrifugal force from the Earth's constant rotation. Using the semi-axes described in Table 1, the equation for the ellipsoidal Earth in spherical

coordinates are given by:

$$\frac{r^2\sin^2\theta_E\cos^2\phi_E}{r_e^2}+\frac{r^2\sin^2\theta_E\sin^2\phi_E}{r_e^2}+\frac{r^2\cos^2\theta_E}{r_p^2}=1 \tag{5}$$

In Equation 5, θ_e is the polar angle, the inclination, and ϕ_e is the azimuthal angle between the orthogonal projection of the r onto the reference positive x-y-plane within the equator. With the introduction of an ellipsoidal Earth model, the approximation of the atmospheric density becomes more complicated. This is due to the requirement for a new method of calculating the height in reference to its distance from the Earth's surface, which is no longer as simple of subtracting the radius of the Earth from the satellites radius of orbit, demonstrated in Figure 2. There was not a tractable analytical solution to calculating this height that the team could find, thus Newton's optimisation routine was implemented. Notice that when converting to 2D Cartesian coordinates angle ϕ_E can be discounted as the initial guess is the satellite vector and changing ϕ_E won't yield a negative change in the distance therefore $(r,\theta_E,\cancel{\phi_E}) \rightarrow (x_p, y_p)$. [6]

$$S_0 = \left(r_e\cos(\theta), r_p\sin(\theta)\right) \tag{6}$$

$$S_i{}' = \left(-r_e\sin(\theta), r_p\cos(\theta)\right) \tag{7}$$

$$S_i{}'' = \left(-r_e\cos(\theta), -r_p\sin(\theta)\right) \tag{8}$$

$$\theta_0 = \arctan 2\left(x_p, y_p\right) \tag{9}$$

$$\theta_{i+1} = \theta_i - \frac{S_i{}'(\theta_i)}{S_i{}''(\theta_i)} \tag{10}$$

$$\text{err} = \left|\frac{\Delta S_i{}'(\theta_i)}{\Delta S_i{}''(\theta_i)}\right| \tag{11}$$

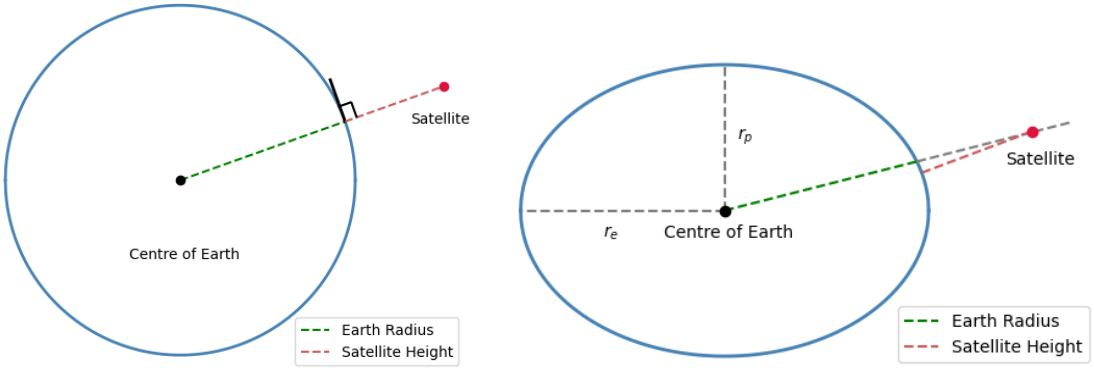

Fig. 2 Height of Satellite for different Earth models (not to scale)

2.4 Atmosphere Model

In order to accurately model the motion of a de-orbiting satellite over time the choice of atmosphere model affects how accurate the predicted drag acting on the satellite is. For a simple model this density can be approximated using the barometric formula with constants:

- R Universal gas constant 8.3144598 N m mol^{-1}K^{-1}

- G Gravitational acceleration 9.0665 m s^{-2}
- m_a Molar mass of Earth's air 0.0289644 kg mol^{-1}

$$\rho(h) = \rho_b \exp\left(-\frac{h-h_b}{H}\right), \quad \text{with } H = \frac{RT_b}{m_a G} \tag{12}$$

The model used for this project is comprised of 34 layers using data from the U.S. Standard Atmosphere [1] for the reference temperature (K) and density (kg m^{-3}) values for each layer b, and for heights between 175 km and 500 km defaults to a single scale height formula presented by Fiolhais, M. et al in [2].

2.5 Extended Kalman Filter

The EKF functions within the satellite's coordinate system, as it applies the 2D dynamics outlined in Section 2.1. Due to the non-linearity in the chosen dynamics; such as the atmospheric drag; the EKF was chosen in favour of the Linear Kalman Filter (LKF), since it approximates these non linearity through calculating a state matrix at each time step. In the steps outlined below the equations are defined within the satellite's coordinate system (r, ϕ_S, θ_S) however for a more comprehensible outline of the theory behind it the S subscript will be dropped. Owing to the fact that the orbital inclination is constant and known the EKF states are only reliant on (r, ϕ_S) [3], when forecasting trajectory.

1. **State Vector Initialisation:** The initial state vector $\mathbf{x}$ includes position, velocity, and acceleration components for both radial and angular dimensions:

$$\mathbf{x}_0 = \begin{bmatrix} r & v_r & \dot{v_r} & \phi & v_\phi & \dot{v_\phi} \end{bmatrix}^T$$

2. **Equations:** For the given model, the radial and angular update calculations are based on current state and physical dynamics:

$$r^{i+1} = r^i + \Delta t\, v_r^i \tag{13}$$

$$v_r^{i+1} = v_r^i + \Delta t\, \dot{v}_r^i \tag{14}$$

$$\dot{v}_r^{i+1} = -\frac{GM_E}{(r^i)^3} + \frac{(v_\phi^i)^2}{(r^i)^2} \tag{15}$$

$$\phi^{i+1} = \phi^i + \frac{\Delta t\, v_\phi^i}{r^i} \tag{16}$$

$$v_\phi^{i+1} = v_\phi^i + \Delta t\, \dot{v}_\phi^i \tag{17}$$

$$\dot{v}_\phi^{i+1} = -\frac{1}{2}\rho^i (v_\phi^i)^2\, B + \frac{v_\phi^i\, v_r^i}{r^i} \tag{18}$$

3. In the aforementioned model the drag density is given by Equation 19. The nonlinear, piece-wise continuous function is an extrapolated table of know values for the density of the atmosphere given it's distance from the planet's surface.

$$\rho^i = f(r^i, \phi^i) \tag{19}$$

4. **State Transition Matrix F:** The calculation of the Jacobian F with respect to the state variables, crucial for the prediction step in the EKF is given by:

$$F_i = \begin{bmatrix} 1 & \Delta t & 0 & 0 & 0 & 0 \\ 0 & 1 & \Delta t & 0 & 0 & 0 \\ \frac{2GM_E}{r^3} - (\frac{v_\phi}{r})^2 & 0 & 0 & 0 & \frac{2v_\phi}{r} & 0 \\ \frac{-\Delta t\, v_\phi}{r^2} & 0 & 0 & 1 & \frac{\Delta t}{r} & 0 \\ 0 & 0 & 0 & 0 & 1 & \Delta t \\ \frac{-v_\phi\, v_r}{r^2} & \frac{v_\phi}{r} & 0 & 0 & -\rho\, v_\phi\, B + \frac{v_r}{r} & 0 \end{bmatrix}$$

5. **Prediction Step:**

   - **State Prediction:** Update the state estimate using the dynamics equations.
   - **Covariance Prediction:** Update the covariance matrix estimate using the discretised Jacobian:

$$\mathbf{P}^{i+1} = \mathbf{F}_i \mathbf{P}^i \mathbf{F}^i.T + \mathbf{Q} \tag{20}$$

     where **Q** is the process noise covariance matrix.

6. **Measurement Update (Measurements of r and ϕ):**

   The values of H reduce to a binary matrix of its linear counterpart as all the observations are prepossessed into the working coordinates of the EKF.

$$\mathbf{H} = \begin{bmatrix} 1 & 0 & 0 & 0 & 0 & 0 \\ 0 & 0 & 0 & 1 & 0 & 0 \end{bmatrix} \tag{21}$$

   - **Kalman Gain K:**

$$\mathbf{K}^i = \mathbf{P}^i \mathbf{H}^T (\mathbf{H}\mathbf{P}^i \mathbf{H}^T + \mathbf{R})^{-1} \tag{22}$$

     where **H** is the measurement matrix, and **R** is the measurement noise covariance.

   - **Update State Estimate:**

$$\mathbf{x}^{i+1} = \mathbf{x}^i + \mathbf{K}^i (\mathbf{y}^i - h(\mathbf{x}^i)) \tag{23}$$

   - **Update Covariance Estimate:**

$$\mathbf{P}^{i+1} = (\mathbf{I} - \mathbf{K}^i \mathbf{H}) \mathbf{P}^i \tag{24}$$

     where **I** is the identity matrix.

3 Program Features

The program orchestrates a comprehensive system for simulating, tracking, and estimating the state of satellites orbiting the Earth. It integrates various modules, including Earth representation, filtering techniques, simulation engines, radar systems, and satellite dynamics modelling.

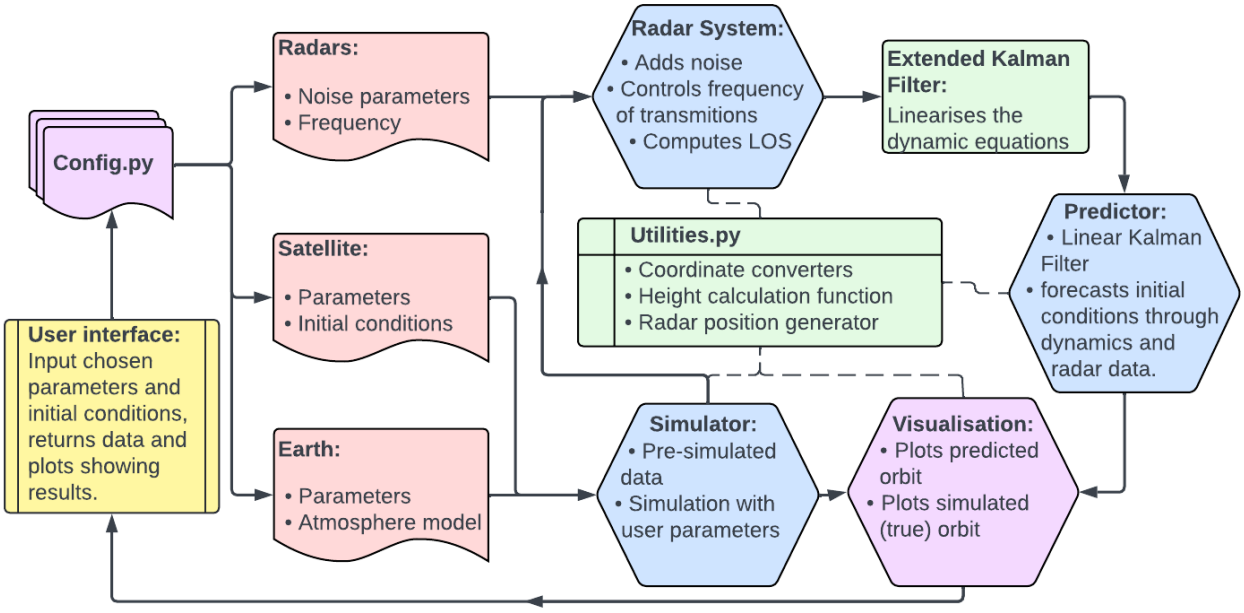

Fig. 3 Flow chart outlining features of the program

The Configuration file contains the properties of the radar system, Earth's constant and the satellite constant for easy and consistent referral across all files.

The Earth module encapsulates properties of the Earth's shape and atmosphere, enabling calculations such as the ellipse equation and air density at different distances.

The Predictor is comprised of the EKF which facilitates accurate estimation of satellite states by linearising non-linear dynamics through a second order approximation, then passing these to the LKF.

The Simulator module offers interfaces for simulating satellite positions in real-time, crucial for debugging and operational simulations.

The Radar system manages the detection and tracking of the satellite by determining line-of-sight visibility and adding noise to detected positions.

The Satellite module models satellite dynamics, including trajectory simulation, state estimation using Kalman filters, and coordinate conversions between Earth's spherical system and the satellite's

spherical systems.

This integrated system provides a versatile framework for analysing satellite trajectories, estimating their states, and facilitating radar-based tracking operations. This flow of code is illustrated with Figure 3.

4 Uncertainty Quantification

The physical simulation in the simulator inherently carries uncertainties due to various factors such as atmospheric drag, solar radiation pressure, and gravitational perturbations from other celestial bodies. Uncertainties in parameters such as satellite mass, shape, and orientation can also affect the simulation results however, these are purposefully kept constant in order to simplify the problem.

The predictor receives radar data, which is noisy and infrequent. The noise in the data introduces uncertainty in the observations of the satellite's position. In addition to sensor noise, uncertainties in the radar's calibration and alignment can further contribute to prediction errors. The predictor needs to incorporate these uncertainties into its estimation process to provide meaningful predictions. This is where the Kalman filter's steps in and takes the reins, steering the predictions in the right direction. Uncertainties in the atmospheric density and other environmental factors affecting the satellite's motion are neglected. The additive nature of noise propagation reduces relevance of additional sources of environmental noise, since measurement noise can be increased to factor this.

5 Results and Discussion

The results of the study reveal a nuanced understanding of the predictive capabilities of the Kalman filter within the integrated system. Initially, without incoming data, the filter's predictions exhibit variability and inconsistency, reflecting the inherent uncertainty in estimating satellite states in the absence of observational input. However, once data streams are introduced into the system, the filter adapts and refines its predictions, showcasing its ability to assimilate new information and converge towards accurate state estimates. Consequently, despite the availability of multiple radars, only a select subset (at most 5%-10%) have line of sight at any given time. The rapid convergence of the covariance matrix from an originally extremely agnostic state is evident from the Figure 4 below. Instances of diverging positional variance were present only as a result of no radar sending data.

The evaluation of predictions across various scenarios, including changes in the number of radars and initial satellite positions as well as increased noise in radial distance and azimuthal angle measurements, demonstrates consistent and reliable performance in estimating both properties. Whilst not all the plau-

sible orbits were stable due to the chaotic nature of the EKF and celestial movement, all reasonable starting conditions of the satellite remaining in Earth's orbit (with a non-zero number of effective observing radars) results in the correct convergence of the satellite trajectory.

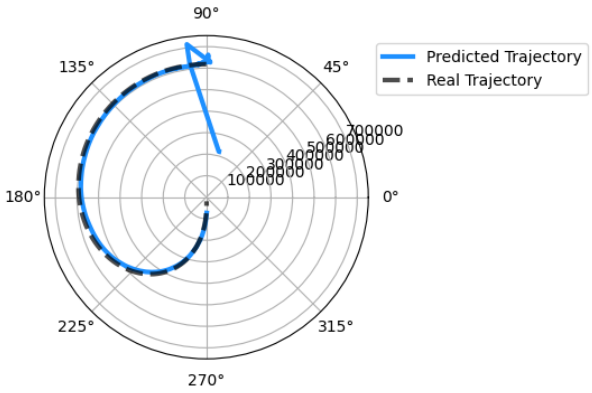

(a) Polar angle vs radius

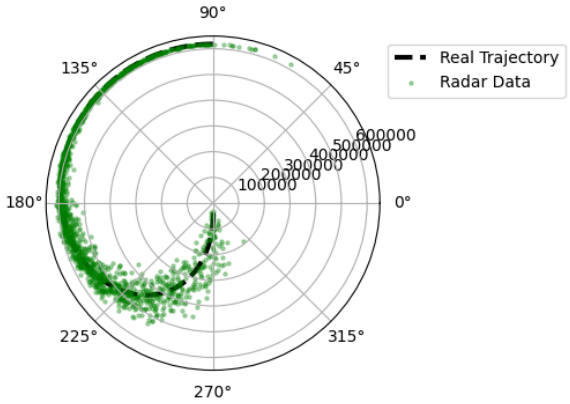

(b) Radar data with noise

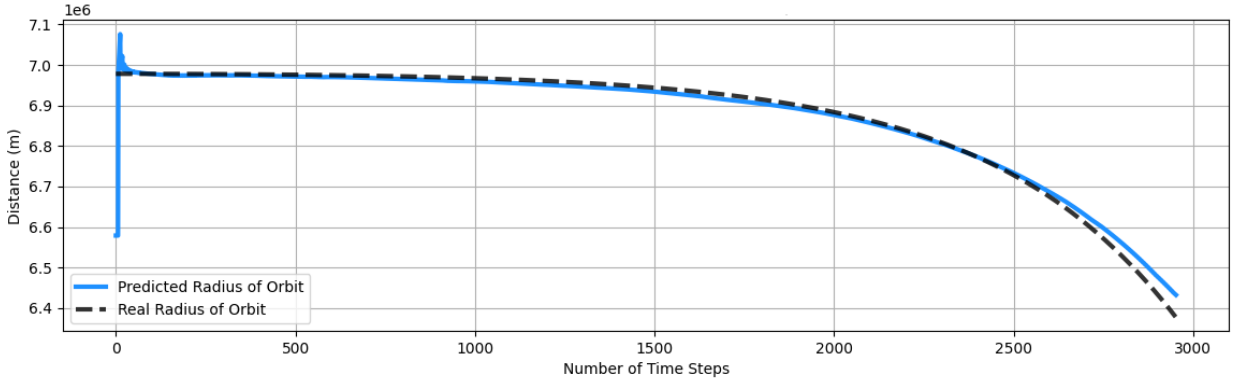

(c) Real vs Predicted radius of orbit

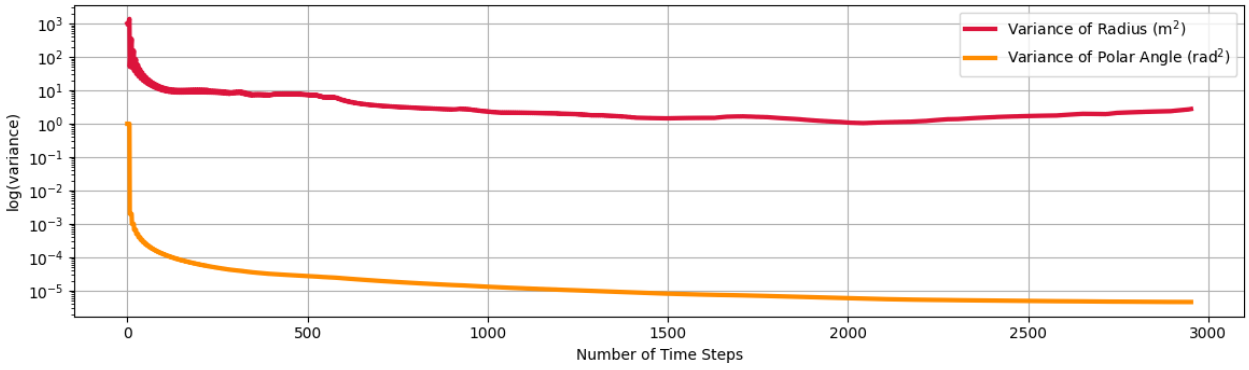

(d) Kalman filter variance

Fig. 4 Uncertainty estimates

References

[1] Center, N. G. D. (1992). U.S. standard atmosphere (1976). , 40(4):553–554.

[2] Fiolhais, M., Gonzalez-Urbina, L., Milewski, T., Chaparro, C., and Ferroglia, A. (2023). Orbital decay in the classroom. *The Physics Teacher*, 61(3):182–185.

[3] Labbe, R. (2022). Kalman and bayesian filters in python. `https://github.com/rlabbe/Kalman-and-Bayesian-Filters-in-Python/blob/master/11-Extended-Kalman-Filters.ipynb` [Accessed: (2024-05-07)].

[4] Nwankwo, V. and Chakrabarti, S. (2014). Theoretical model of drag force impact on a model international space station satellite due to solar activity. *TRANSACTIONS OF THE JAPAN SOCIETY FOR AERONAUTICAL AND SPACE SCIENCES SPACE TECHNOLOGY JAPAN*, 12:47–53.

[5] Pardini, C. and Anselmo, L. (2019). Monitoring the orbital decay of the chinese space station tiangong-1 from the loss of control until the re-entry into the earth's atmosphere. *Journal of Space Safety Engineering*, 6(4):265–275.

[6] Pewsey, M. (2022). Minimum distance between ellipse and point. `https://mpewsey.github.io/2021/11/07/minimum-distance-between-ellipse-and-point.html` [Accessed: (2024-05-14)].